Frontiers of Information Technology & Electronic Engineering
www.zju.edu.cn/jzus; engineering.cae.cn; www.springerlink.com
ISSN 2095-9184 (print); ISSN 2095-9230 (online)
E-mail: jzus@zju.edu.cn

Micro-angle tilt detection for the rotor of a novel rotational gyroscope with a 0.47″ resolution*

Hai LI[1], Xiao-wei LIU[1,2], Rui WENG[2], Hai-feng ZHANG[†‡1,2]

([1]*MEMS Center, Harbin Institute of Technology, Harbin 150001, China*)

([2]*MOE Key Laboratory of Micro-Systems and Micro-Structures Manufacturing, Harbin 150001, China*)

[†]E-mail: zhanghf@hit.edu.cn

Received Dec. 11, 2015; Revision accepted Mar. 20, 2016; Crosschecked Apr. 27, 2017

Abstract: Differential capacitive detection has been widely used in the displacement measurement of the proof mass of vibratory gyroscopes, but it did not achieve high resolutions in angle detection of rotational gyroscopes due to restrictions in structure, theory, and interface circuitry. In this paper, a differential capacitive detection structure is presented to measure the tilt angle of the rotor of a novel rotational gyroscope. A mathematical model is built to study how the structure's capacitance changes with the rotor tilt angles. The relationship between differential capacitance and structural parameters is analyzed, and preliminarily optimized size parameters are adopted. A low-noise readout interface circuit is designed to convert differential capacitance changes to voltage signals. Rate table test results of the gyroscope show that the smallest resolvable tilt angle of the rotor is less than 0.47″ (0.00013°), and the nonlinearity of the angle detection structure is 0.33%, which can be further improved. The results indicate that the proposed detection structure and the circuitry are helpful for a high accuracy of the gyroscope.

Key words: Micro-angle detection; Differential capacitive structure; Rotational gyroscope; Structure optimization
http://dx.doi.org/10.1631/FITEE.1500454 **CLC number:** TP212.1

1 Introduction

As an important sensor of the inertial navigation system, gyroscopes have been widely used to measure the angular rates of their carriers. Conventional rotational gyroscopes have been proven to have the ability to achieve high precision, but they are hard to manufacture and bulky (Hays *et al.*, 2002). Microelectro-mechanical systems (MEMS) gyroscopes are small and cheap, but their accuracy is low and difficult to improve (Liu *et al.*, 2009; 2015; Challoner *et al.*, 2014). This paper presents a novel rotational gyroscope that has a simpler structure and a smaller volume compared to conventional rotational gyroscopes and has the potential to achieve better performance than general MEMS gyroscopes (Li *et al.*, 2014).

The structure of the proposed gyroscope is shown in Fig. 1. It is composed mainly of a rotor, a stator, two supporting frames, and 12 exciting coils. The rotor has a ball-disk structure, making a spherical joint together with two frames, which provides the rotor three rotational degrees of freedom (DOFs). The rotor spins at a high speed, driven by the spinning magnetic field generated by the coils on the stator. According to the law of conservation of angular momentum, when there is a constant angular velocity perpendicular to the rotating axis of the rotor, the rotor tilts away from its null position. It will finally stay at a constant angle under the

‡ Corresponding author

* Project supported by the National Natural Basic Research Program (973) of China (No. 2012CB934104), the National Natural Science Foundation of China (No. 61071037), and the Natural Science Foundation of Heilongjiang Province, China (No. F201418)

ORCID: Hai-feng ZHANG, http://orcid.org/0000-0002-4917-746X

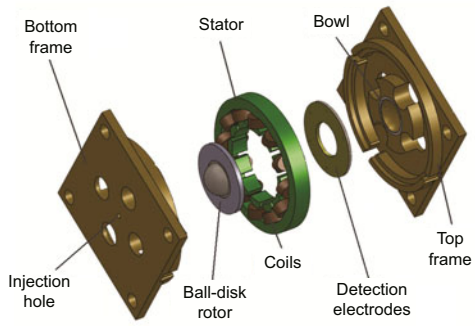

Fig. 1 Assembly drawing of the mechanical structure of the gyroscope

influence of magnetic and damping torques. By detecting the tilt angle of the rotor, the input angular velocity can be determined. To achieve a high resolution of the gyroscope, very small angle changes of the rotor must be determined, which places high requirements on the angle detection.

Differential capacitive detection has been widely used in the displacement measurement of the proof of mass of vibratory gyroscopes because of its advantages of non-contact measurement, ease of fabrication, low power consumption, etc. (Shearwood *et al.*, 2000; Xia *et al.*, 2015). They are successful in converting small displacement into large capacitance changes (Liu *et al.*, 2009). However, little has been reported on the angle measurement of gyroscopes using differential capacitive detection (Xia *et al.*, 2014). Houlihan and Kraft (2002) presented a differential capacitor structure and built a model for a single capacitor as a function of the tilt angle of the rotor of a rotational gyroscope. However, the difference of the capacitance changes of the same pair was not modeled, which takes a simpler form as will be discussed later. Huang *et al.* (2007) at Shanghai Jiao Tong University, China constructed a similar structure for the angle detection of their rotational gyroscope, and the detection circuit achieved an angular resolution of 0.04° with a nonlinearity error of 2.3%, which should be improved to make the gyroscope competitive. Besides, the detecting capacitors in these levitated rotational gyroscopes are a series of two capacitors, which greatly reduces the capacitance and leads to small structural sensitivities (Liu *et al.*, 2008; Tsai *et al.*, 2009).

Interface circuitry is another important part of a gyroscope. The majority of MEMS gyroscopes adopt the twice-modulation detection methods (Alper *et al.*, 2008; Aaltonen and Halonen, 2010). The input signal of the gyroscope is first modulated by the drive oscillation with a relatively low frequency (several kilohertz), which keeps the mass vibrating along the driving direction. The signal is then modulated by the sense oscillation with a high frequency (usually more than 100 kHz) for the detection of the capacitance change. In a typical open-loop detection circuit, the sensor outputs are converted to voltage signals by preamplifier stages, and a low-frequency output is obtained proportional to the applied angular rate input after twice demodulation and low-pass filtering (Xia *et al.*, 2014). These circuits have to adopt denoising techniques in the drive and sense frequency bands to achieve low noise. However, there is no drive modulation in the proposed gyroscope, so the conventional sensing structures cannot provide significant suppression to the low-frequency noise of this system (Feng *et al.*, 2011; Fang *et al.*, 2012). Several institutions have reported similar Σ-Δ interface circuits for the sensing of electrostatic suspension rotational micro-gyroscopes (Gindila and Kraft, 2003; Murakoshi *et al.*, 2003; Damrongsak and Kraft, 2006). However, the structures require a full closed-loop control of the rotor with a non-contact force, which does not apply to the gyroscope discussed in this paper. Huang *et al.* (2007) also proposed a printed circuit board (PCB) detection circuit using discrete components; capacitance changes are converted into voltage signals with integral charge amplifiers and the output is obtained after direct demodulation and a two-order low-pass filtering. The circuit noise was modeled in detail, but no special measures were taken to reduce low-frequency noise.

In this paper, a special differential capacitive detection structure is presented, and an application-specific integrated circuit (ASIC) is designed to measure the small tilt angle of the rotor. A mathematical model is built to study how the structure's capacitance changes with the rotor tilt angle. Rate table test results of the gyroscope show that the angle can be detected with a high resolution.

2 Angle detection structure

A detection board, with four electrodes on its surface, is inserted between the rotor and the top frame, to detect the small tilt angle of the rotor on

its two radial axes (Fig. 2a). Each electrode forms a capacitor with the rotor, and two capacitors on the X axis form a pair of differential capacitors C_{X+} and C_{X-} and the same with C_{Y+} and C_{Y-} (Fig. 2b). The rotor acts as one pole of the capacitors, which is different from similar structures presented in the levitated rotational gyroscopes that use additional electrodes as the other pole of the capacitors. This characteristic makes it easier to achieve a larger sensitivity than the structures presented in Houlihan and Kraft (2002) and Huang *et al.* (2007), because there is no capacitance reduction due to the series connection of two capacitors and area occupied by additional electrodes.

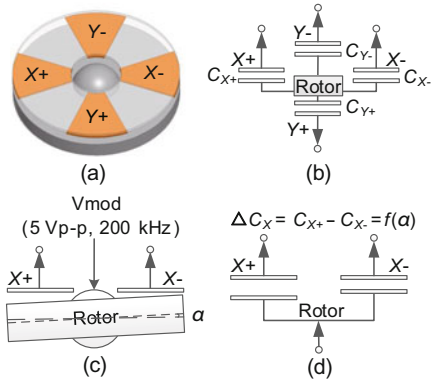

Fig. 2 Schematic of the micro-angle detecting structure (a) and its equivalent circuit (b), and schematic of the detection structure when the rotor tilts away from its null position (c) and its equivalent circuit (d)

The capacitances can be calculated by the capacitance formula for parallel-plate capacitors, $\varepsilon S/h$, where ε is the permittivity of the air between two plates, and S and h are the overlapping surface area and the gap between them, respectively. The capacitance of a capacitor is inversely proportional to the gap between its two plates. When the rotor tilts away from its null position (Fig. 2c), the gaps between the rotor and the detecting electrodes change, thereby causing a change in the detecting capacitance as well.

For a differential capacitor pair C_{X+} and C_{X-}, the equivalent gap changes between them are of the same value but opposite signs because of the symmetrical structure. The differential capacitance ΔC of the differential capacitor pair C_{X+} and C_{X-} can be calculated as

$$\Delta C_X = C_{X+} - C_{X-} = \frac{\varepsilon S}{h_{X+}} - \frac{\varepsilon S}{h_{X-}}, \qquad (1)$$

where h_{X+} and h_{X-} are the equivalent distances from the $X+$ and $X-$ poles to the rotor surface, respectively, and they are both functions of the tilt angle α (Fig. 2d). Thus, the differential capacitance is a function of the tilt angles, and a model is necessary to fully understand their relationship.

3 Modeling of differential capacitance

The structural parameters of $X+$ and $X-$ poles are shown in Fig. 3, where θ_0 is half the arc angle of the electrodes, R_i is the inner radius of the electrodes, and R_o is the outer radius of the electrodes. α and β are the tilt angles of the rotor about Y-axis and negative X-axis, respectively.

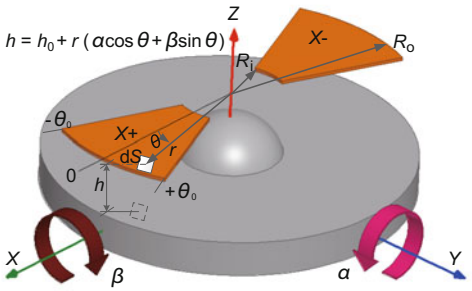

Fig. 3 The differential capacitor pair formed by electrodes $X+$ and $X-$ with the rotor where the capacitances are functions of the tilt angles of the rotor (References to color refer to the online version of this figure)

The capacitance C_{X+} can be calculated by

$$\begin{aligned} C_{X+} &= \iint \varepsilon \frac{\mathrm{d}S}{h} \\ &= \varepsilon \int_{-\theta_0}^{+\theta_0} \int_{R_\mathrm{i}}^{R_\mathrm{o}} \frac{r\mathrm{d}\theta\mathrm{d}r}{h_0 + r(\alpha\cos\theta + \beta\sin\theta)} \\ &= \varepsilon \int_{-\theta_0}^{+\theta_0} \int_{R_\mathrm{i}}^{R_\mathrm{o}} \frac{r\mathrm{d}\theta\mathrm{d}r}{h_0 + r\kappa(\theta)}, \end{aligned} \qquad (2)$$

where h_0 is the gap when the rotor is at null position, and $\kappa(\theta) = \alpha\cos\theta + \beta\sin\theta$ (Houlihan and Kraft, 2002). Integrating Eq. (2) along r gives

$$\begin{aligned} C_{X+} = \varepsilon \int_{-\theta_0}^{+\theta_0} \Bigg\{ & \frac{R_\mathrm{o} - R_\mathrm{i}}{\kappa(\theta)} \\ & - \frac{h_0\left[\ln(R_\mathrm{o}\kappa(\theta) + h_0) - \ln(R_\mathrm{i}\kappa(\theta) + h_0)\right]}{\kappa^2(\theta)} \Bigg\} \mathrm{d}\theta. \end{aligned} \qquad (3)$$

The difference of the two logarithmic terms in Eq. (3) is expanded using a Taylor series to find

an analytical expression for C_{X+}. The expansion is given as follows:

$$\ln(R_o\kappa(\theta)+h_0)-\ln(R_i\kappa(\theta)+h_0)=\sum_{n=1}^{\infty}(-1)^{n+1}\frac{R_o^n-R_i^n}{nh_0^n}\kappa^n(\theta). \quad (4)$$

By inserting Eq. (4) into Eq. (3) and simplifying Eq. (3), we obtain

$$C_{X+}=\varepsilon\int_{-\theta_0}^{+\theta_0}\sum_{n=2}^{\infty}(-1)^n\frac{R_o^n-R_i^n}{nh_0^{n-1}}\kappa^{n-2}(\theta)\mathrm{d}\theta. \quad (5)$$

C_{X-} is different from C_{X+} only in the angle limitation of integration, and can be calculated as

$$\begin{aligned}C_{X-}&=\varepsilon\int_{-\theta_0}^{+\theta_0}\int_{R_i}^{R_o}\frac{r\mathrm{d}\theta\mathrm{d}r}{h_0-r(\alpha\cos\theta+\beta\sin\theta)}\\&=\varepsilon\int_{-\theta_0}^{+\theta_0}\int_{R_i}^{R_o}\frac{r\mathrm{d}\theta\mathrm{d}r}{h_0-r\kappa(\theta)}.\end{aligned} \quad (6)$$

We can deduce the formula of C_{X-} by the same way as in the case of C_{X+}. It takes the form

$$C_{X-}=\varepsilon\int_{-\theta_0}^{+\theta_0}\sum_{n=2}^{\infty}\frac{R_o^n-R_i^n}{nh_0^{n-1}}\kappa^{n-2}(\theta)\mathrm{d}\theta. \quad (7)$$

The differential capacitance ΔC_X can be calculated as

$$\Delta C_X=-2\varepsilon\sum_{\substack{n=2N+1\\N=1}}^{N=\infty}\frac{R_o^n-R_i^n}{nh_0^{n-1}}\int_{-\theta_0}^{+\theta_0}\kappa^{n-2}(\theta)\mathrm{d}\theta. \quad (8)$$

By polynomial expansion and induction, we obtain Eq. (9) (at the bottom of this page).

The differential capacitance is a polynomial function of the tilt angles and does not contain even-degree terms. The expansion of Eq. (9), with its first- and third-degree terms shown, is as follows:

$$\Delta C_X=-4\varepsilon\frac{R_o^3-R_i^3}{3h_0^2}\alpha\sin\theta_0-4\varepsilon\frac{R_o^5-R_i^5}{15h_0^4}\cdot\left[(\cos^2\theta_0+2)\alpha^3\sin\theta_0+3\alpha\beta^2\sin^3\theta_0\right]-\cdots. \quad (10)$$

We can conclude from Eq. (10) the following: (1) Increasing R_o or decreasing R_i can increase the sensitivity, but the nonlinearity will be increased as well; (2) Increasing the gap h_0 helps reduce the nonlinearity, but will reduce the sensitivity; (3) Increasing θ_0 helps improve the sensitivity and may affect the nonlinearity, but θ_0 cannot be larger than 45°. Besides, due to the size limitation of the gyroscope, R_i and R_o are almost fixed, and the gap h_0 is set to be 200 μm to maintain a full scale of ±100°/s of the gyroscope at 10 000 r/min. However, θ_0 is relatively free for optimization. Fig. 4 shows the sensitivity and nonlinearity of the detection structure as functions of θ_0 according to Eq. (9), when the maximum tilt angle is 2° as determined by the structure parameters. It indicates that when θ_0 increases, the sensitivity increases and the nonlinearity error decreases. So, a large θ_0 should be taken. Here, we adopt 43° instead of the maximum value 45° to reduce cross-coupling from adjacent poles.

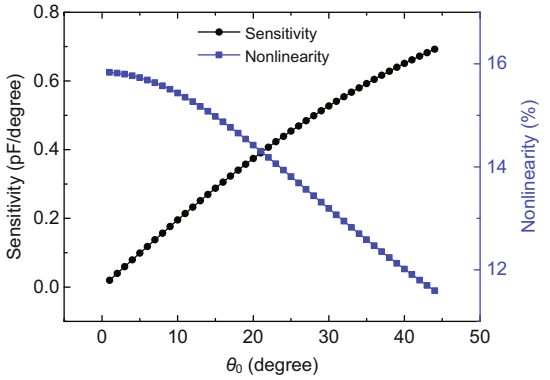

Fig. 4 Structure sensitivity and nonlinearity as functions of θ_0 when R_i, R_o, and h_0 are 2 mm, 5 mm, and 200 μm, respectively. The maximum tilt angle is 2° determined by the structure parameters

Taking the above aspects into consideration, the following optimized structure parameters are adopted: R_i = 2 mm, R_o = 5 mm, h_0 = 200 μm, and θ_0 = 43°. For these structural parameters, the crosstalk from the orthogonal direction is less than

$$\Delta C_X=-4\varepsilon\sum_{\substack{n=2M+1\\M=0}}^{M=\infty}\frac{R_o^{n+2}-R_i^{n+2}}{n(n+2)h_0^{n+1}}\sum_{\substack{k=2N+1\\N=0}}^{N=\frac{n-1}{2}}\binom{n}{n-k}\sin^{n-k+1}\theta_0\cos^{k-1}\theta_0\cdot\left[1+\sum_{l=1}^{l=\frac{k-1}{2}}\left(\prod_{m=0}^{m=l-1}\frac{k-1-2m}{n-2-2m}\right)\cos^{-2l}\theta_0\right]\alpha^k\beta^{n-k}. \quad (9)$$

5.62% of the differential capacitance when the tilt angle is limited within $\pm 1°$ (the design aim of the full scale of angle detection), and can be reduced by compensation. Thus, we ignore the crosstalk effect when evaluating the detection structure to simplify the analysis by assuming that the angle in one direction is always zero. The differential capacitances are calculated as functions of α ($\beta = 0$), according to Eq. (9) when n takes different values, compared to numerical integration results (Fig. 5).

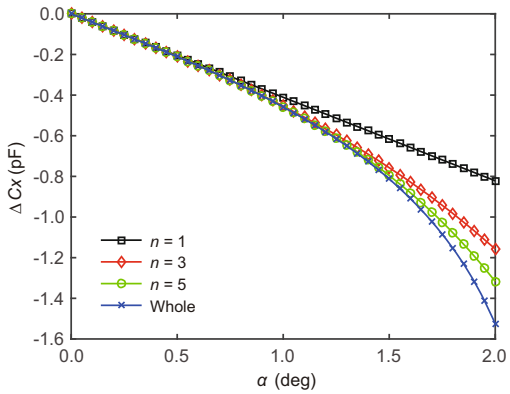

Fig. 5 Comparison of differential capacitances as functions of α between calculation results ($n = 1, 3, 5$) and numerical integration (R_i, R_o, h_0, and θ_0 are 2 mm, 5 mm, 200 μm, and 43°, respectively)

Fig. 5 shows that the values of the first-degree term of Eq. (9) are close enough to those of the numerical integration when the tilt angle is small (within 0.5°), but as the angle increases, the error enlarges significantly. Better approximations can be made by increasing the polynomial orders and constraining the measuring range, but polynomials of orders equal to or more than five cannot be solved by equations, which makes the calculation of the gyroscope difficult. Taken together, a cubic polynomial fitting can be applied if the maximum tilt angle at a full-scale input condition is limited within $\pm 1°$ by controlling the gyroscope's operating parameters, such as rotating speed (Xia *et al.*, 2014).

4 Experimental results

4.1 Design and test of the interface circuit

The circuit design is very important for a gyroscope to realize a high accuracy. Normally, different gyroscope structures require different circuits (Xia *et al.*, 2014). ASICs have the advantage of a higher performance than PCB circuits in specific conditions such as bandwidth, because much better parameter optimizations can be made to the components of ASICs. An ASIC with continuous-time (CT) topology is designed for capacitance-voltage conversion and to acquire a low noise level (Sung *et al.*, 2008; Northemann *et al.*, 2010; Xu *et al.*, 2015). The schematic of the detecting circuit is shown in Fig. 6.

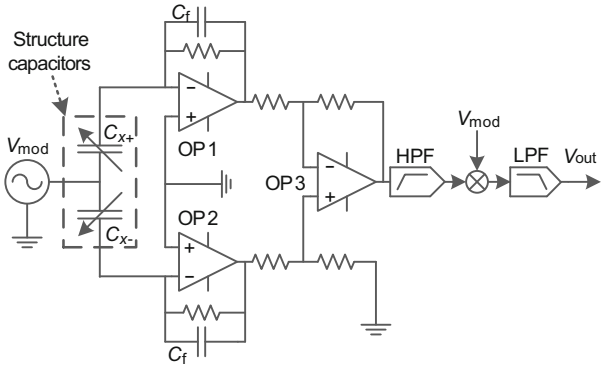

Fig. 6 Schematic of the detection circuit

The changes of detection capacitances are modulated to a high frequency by a sinusoidal signal imposed to the rotor and are converted to voltage signals by charge amplifiers. A differential amplifier structure is constructed to amplify the difference of two voltage signals from the two charge amplifiers. A high-pass filter (HPF) is used to suppress low-frequency noise generated in the previous circuit. After demodulation and low-pass filtering, the changes of the differential capacitances are converted to voltage signals ready to be processed by a digital signal processor. The detection board is shown in Fig. 7a, and the ASIC is shown in Fig. 7b.

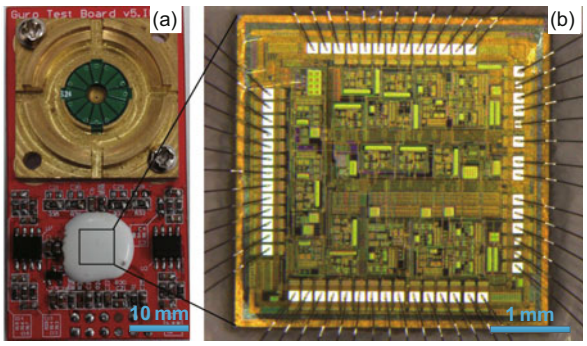

Fig. 7 Detection board (a) and micrograph of the readout ASIC (b)

The capacitance of the feedback capacitor is designed to be 3 pF, and a discrete 200 MΩ resistor is connected parallel to each feedback capacitor on the PCB to prevent the capacitor from breaking down. The modulation signal is sinusoidal with a 200-kHz frequency and a 2-Vp-p magnitude. The HPF is a two-stage second-order Butterworth HPF with a cut-off frequency of about 2 kHz, and the low-pass filter (LPF) is a two-stage second-order Butterworth LPF with a cutoff frequency of 20 Hz. The power voltages are ±9 V, and the working current of the detection circuit is below 25 mA. The static noise of the detection circuit with the capacitors connected and the rotor stopped is measured with a spectrum analyzer (Fig. 8).

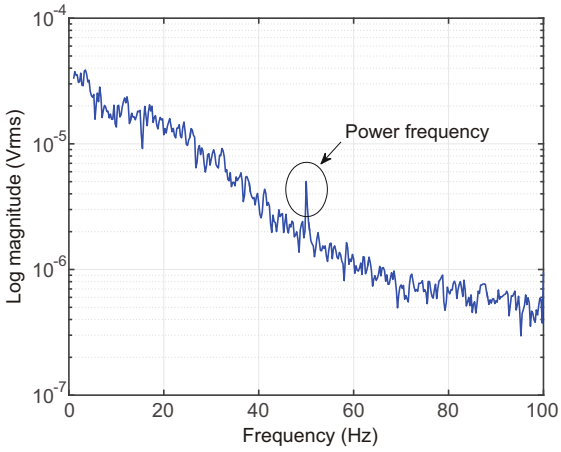

Fig. 8 Static output noise of the detection circuit

There is a large power frequency interference since the circuit is measured directly in the laboratory, but this can be suppressed greatly by electromagnetic shielding (Lam *et al.*, 2003). The spectrum takes the form of $1/f$ noise at the very beginning, and then the noise shape of a LPF after about 10 Hz. The static output noise of the detection circuit is now 35 $\mu V/\sqrt{Hz}$ at the frequency of 1 Hz. The broadband noise floor is about 15 $\mu V/\sqrt{Hz}$ in the band of the gyroscope, which is within 20 Hz.

4.2 Gyroscope test

A prototype of the gyroscope structure is shown in Figs. 9a and 9b. The size of the kernel part of the gyroscope is within 6 cm^3. The ball of the rotor has a radius of 1.5 mm, and the inner radius, outer radius, and thickness of the rotor disk are 1.5, 5.0, and 0.8 mm, respectively. The inner radius, outer radius, and arc angle of the electrodes are 2 mm, 5 mm, and 86°, respectively. The gap between the rotor and the sensing electrodes is designed to be 200 μm. It needs only 0.75 W to keep the rotor spinning at the speed of 15 000 r/min. The gyroscope is tested on a rate table at an ambient temperature of 20 °C (Fig. 9c).

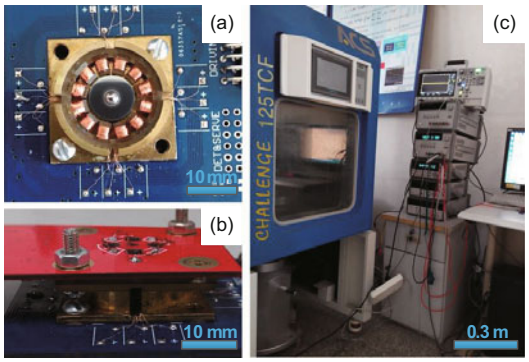

Fig. 9 Driving structure of the gyroscope with its rotor running at 7000 r/min (a), gyroscope structure (b), and the rate table test platform (c)

Fig. 10 shows the static output voltage of the detection circuit with the rotor rotating at 7000 r/min. The measurement is taken from the time the rotor reaches the speed, with a sampling frequency of 5 Hz and time length of 50 min.

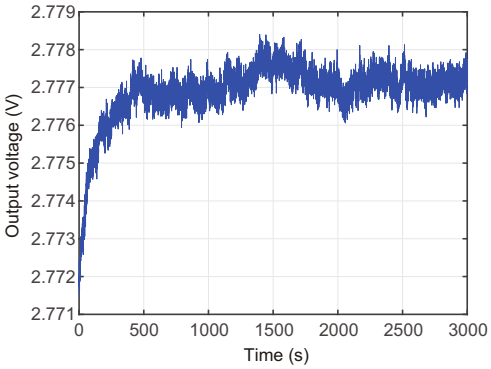

Fig. 10 Static output voltage of the detection circuit with the rotor rotating at 7000 r/min, measured for 50 min after the rotor reaches the speed

The output voltage increases at the beginning, and falls in the range 2.776–2.778 V after several minutes. This is because the working condition of the gyroscope system needs a certain time to stabilize. The maximum peak-to-peak magnitude of the noise is about 1.5 mV (corresponding to a 250-μVrms noise), when the obvious trend is removed. Fig. 11

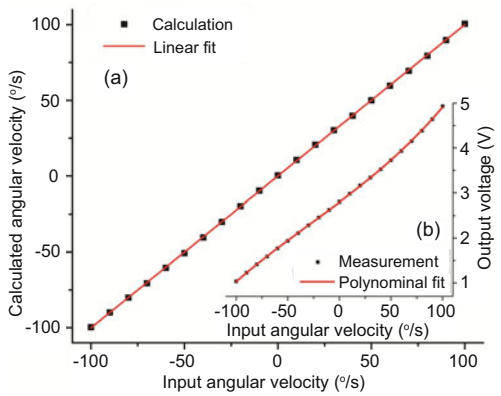

Fig. 11 Calculated angular velocity versus input angular velocity (a) and cubic polynomial fitting of the stable detection circuit output versus input angular velocity (b)

shows the stable gyroscope output in response to input angular velocities varying from −100 to +100°/s at 7000 r/min (Xue *et al.*, 2015).

Fig. 11b shows the cubic polynomial fitting result of the analog voltage output from the detection circuit as a function of the input angular velocity. It indicates that the gyroscope scale factor is greater than 17.3 mV·s/°, and the nonlinearity is about 5.4%. As has been discussed in Section 3, a cubic polynomial fitting is applied to reduce this nonlinearity error. The angular velocities can be calculated by solving the cubic fitting polynomial as a function of the output voltage. The corresponding relationship between the calculated angular velocity and the input angular velocity is shown in Fig. 11a. After this process, the nonlinearity of the gyroscope reaches 0.33%, which can be further reduced by calibration and polynomial fitting of a higher order.

5 Discussions

The 108-μVrms static output noise of the detection circuit is measured within the band of the gyroscope. This noise level is lower than the 250-μVrms result measured when the rotor rotates at 7000 r/min, because the rotor rotating measurement takes the interferences of the power line, the driving frequencies, and the temperature effect into account. These interferences can be further reduced through shielding, digital processing, and temperature control, respectively. When divided by the gyroscope scale factor 17.3 mV·s/°, an input angular rate resolution of about 0.0063°/s is obtained. According to the full scale (±100°/s) and the maximum tilt angle (less than ± 2°), when the circuit is used to provide a readout for the gyroscope with 20 Hz bandwidth, the smallest resolvable tilt of the rotor would be less than 0.47″ (about 0.00013°). Theoretically, the resolution can be improved to be 26 micro degrees by increasing the peak-to-peak modulation signal voltage from 2 V to 10 V, although it means a larger output voltage range. The nonlinearity of the angle detection structure is the same as that of the gyroscope, which is below 0.33% (Cui *et al.*, 2004).

The angle detection performances are compared with those in Huang *et al.* (2007). Table 1 shows that we achieve a higher resolution of angle detection (0.00013°) than Huang *et al.* (2007) (0.04°). This is because the proposed differential capacitance structure has a higher structural sensitivity, and the designed CT based ASIC has a better signal-to-noise ratio than the PCB-based circuit. Besides, a better nonlinearity is acquired according to the constructed model, which defines the relationship between the tilt angles and the differential capacitor instead of a single detection capacitor.

Table 1 Comparison of this work and the literature

Reference	Circuitry	Resolution	Nonlinearity
Huang *et al.* (2007)	PCB	0.04°	2.3%
This work	ASIC	0.00013°	0.33%

6 Conclusions

In this paper, a special differential capacitive detection structure was presented to detect the tilt angle of the rotor of a novel rotational gyroscope. A detailed model of the differential capacitance of the detection structure was built and tested. The relationship between differential capacitance and structural parameters was analyzed, and preliminarily optimized size parameters were adopted. A modulation-high-pass filtering-demodulation ASIC was designed to transfer the differential capacitance changes to voltage signals with a broadband noise floor of about 15 $\mu V/\sqrt{Hz}$ for frequencies within 20 Hz. The gyroscope was tested on a rate table with the rotor rotating at 7000 r/min. Test results showed that the smallest resolvable tilt of the rotor was less than 0.47″, and the nonlinearity of the detecting structure reached 0.33%, which can be further improved.

References

Aaltonen, L., Halonen, K.A.I., 2010. An analog drive loop for a capacitive MEMS gyroscope. *Anal. Integr. Circ. Sig. Process.*, **63**(3):465-476. http://dx.doi.org/10.1007/s10470-009-9395-6

Alper, S.E., Temiz, Y., Akin, T., 2008. A compact angular rate sensor system using a fully decoupled silicon-on-glass MEMS gyroscope. *J. Microelectromech. Syst.*, **17**(6):1418-1429. http://dx.doi.org/10.1109/JMEMS.2008.2007274

Challoner, A.D., Ge, H.H., Liu, J.Y., 2014. Boeing disc resonator gyroscope. IEEE/ION Position, Location and Navigation Symp., p.504-514. http://dx.doi.org/10.1109/PLANS.2014.6851410

Cui, F., Chen, W., Su, Y., *et al.*, 2004. Design of electrostatically levitated micromachined rotational gyroscope based on UV-LIGA technology. *SPIE*, **5641**:264-275. http://dx.doi.org/10.1117/12.575632

Damrongsak, B., Kraft, M., 2006. Design and simulation of a micromachined electrostatically suspended gyroscope. IET Seminar on MEMS Sensors and Actuators, p.267-272. http://dx.doi.org/10.1049/ic:20060468

Fang, R., Lu, W., Tao, T., *et al.*, 2012. A control and readout circuit with capacitive mismatch auto-compensation for MEMS vibratory gyroscope. IEEE 11th Int. Conf. on Solid-State and Integrated Circuit Technology, p.1-3. http://dx.doi.org/10.1109/ICSICT.2012.6467587

Feng, L., Zhang, Z., Sun, Y., *et al.*, 2011. Differential pickup circuit design of a kind of Z-axis MEMS quartz gyroscope. *Proc. Eng.*, **15**:999-1003. http://dx.doi.org/10.1016/j.proeng.2011.08.185

Gindila, M.V., Kraft, M., 2003. Electronic interface design for an electrically floating micro-disc. *J. Micromech. Microeng.*, **13**(4):S11-S16. http://dx.doi.org/10.1088/0960-1317/13/4/302

Hays, K., Schmidt, R., Wilson, W., *et al.*, 2002. A submarine navigator for the 21st century. IEEE Position Location and Navigation Symp., p.179-188. http://dx.doi.org/10.1109/PLANS.2002.998906

Houlihan, R., Kraft, M., 2002. Modelling of an accelerometer based on a levitated proof mass. *J. Micromech. Microeng.*, **12**(4):495. http://dx.doi.org/10.1088/0960-1317/12/4/325

Huang, X.G., Chen, W.Y., Liu, W., *et al.*, 2007. High resolution differential capacitance detection scheme for micro levitated rotor gyroscope. *Chin. J. Aeronaut.*, **20**(6):546-551. http://dx.doi.org/10.1016/S1000-9361(07)60080-6

Lam, Q.M., Stamatakos, N., Woodruff, C., *et al.*, 2003. Gyro modeling and estimation of its random noise sources. AIAA Guidance, Navigation, and Control Conf. and Exhibit, p.1-11. http://dx.doi.org/10.2514/6.2003-5562

Li, H., Liu, X., Wang, B., *et al.*, 2014. Impact of assembly on signal detection from thin-wall rotors of micro-gyroscopes. *AIP Adv.*, **4**(3):031341. http://dx.doi.org/10.1063/1.4869618

Liu, J., Shen, Q., Qin, W., 2015. Signal processing technique for combining numerous MEMS gyroscopes based on dynamic conditional correlation. *Micromachines*, **6**(6):684-698. http://dx.doi.org/10.3390/mi6060684

Liu, K., Zhang, W.P., Chen, W.Y., *et al.*, 2009. The development of micro-gyroscope technology. *J. Micromech. Microeng.*, **19**(11):113001. http://dx.doi.org/10.1088/0960-1317/19/11/113001

Liu, W., Chen, W.Y., Zhang, W.P., *et al.*, 2008. Variable-capacitance micromotor with levitated diamagnetic rotor. *Electron. Lett.*, **44**(11):681-683. http://dx.doi.org/10.1049/el:20080528

Murakoshi, T., Endo, Y., Fukatsu, K., *et al.*, 2003. Electrostatically levitated ring-shaped rotational-gyro/accelerometer. *Jpn. J. Appl. Phys.*, **42**(4S): 2468-2472. http://dx.doi.org/10.1143/JJAP.42.2468

Northemann, T., Maurer, M., Rombach, S., *et al.*, 2010. A digital interface for gyroscopes controlling the primary and secondary mode using bandpass sigma-delta modulation. *Sens. Actuat. A*, **162**(2):388-393. http://dx.doi.org/10.1016/j.sna.2010.05.034

Shearwood, C., Ho, K.Y., Williams, C.B., *et al.*, 2000. Development of a levitated micromotor for application as a gyroscope. *Sens. Actuat. A*, **83**(1-3):85-92. http://dx.doi.org/10.1016/S0924-4247(00)00292-2

Sung, W.T., Sung, S., Lee, J.Y., *et al.*, 2008. Development of a lateral velocity-controlled MEMS vibratory gyroscope and its performance test. *J. Micromech. Microeng.*, **18**(5):055028. http://dx.doi.org/10.1088/0960-1317/18/5/055028

Tsai, N.C., Huang, W.M., Chiang, C.W., 2009. Magnetic actuator design for single-axis micro-gyroscopes. *Microsyst. Technol.*, **15**(4):493-503. http://dx.doi.org/10.1007/s00542-008-0769-y

Xia, D., Yu, C., Kong, L., 2014. The development of micromachined gyroscope structure and circuitry technology. *Sensors*, **14**(1):1394-1473. http://dx.doi.org/10.3390/s140101394

Xia, D., Kong, L., Gao, H., 2015. Design and analysis of a novel fully decoupled tri-axis linear vibratory gyroscope with matched modes. *Sensors*, **15**(7):16929-16955. http://dx.doi.org/10.3390/s150716929

Xu, H., Liu, X., Yin, L., 2015. A closed-loop $\Sigma\Delta$ interface for a high-Q micromechanical capacitive accelerometer with 200 $\mathrm{ng}/\sqrt{\mathrm{Hz}}$ input noise density. *IEEE J. Solid-State Circ.*, **50**(9):2101-2112. http://dx.doi.org/10.1109/JSSC.2015.2428278

Xue, L., Jiang, C., Wang, L., *et al.*, 2015. Noise reduction of MEMS gyroscope based on direct modeling for an angular rate signal. *Micromachines*, **6**(2):266-280. http://dx.doi.org/10.3390/mi6020266